Chalcogenide Letters Vol. 21, No. 4, April 2024, p. 305 - 317

Effect of defect density, bandgap profile, material composition, thickness, and doping density of the absorber layer on the performance of thin film solar cell based on antimony selenosulfide $Sb_2(Se_{1-y}S_y)_3$

A. Benmir*, M. L. Louazene
Laboratory of Electrical Engineering (LAGE), Department of Electrical Engineering, Kasdi Merbah University Ouargla, Ouargla 30000, Algeria

This article deals with the optimization by simulation of a graded bandgap thin film solar cell based on antimony selenosulfide $Sb_2(Se_{1-y}S_y)_3$ having the following structure: Front contact/n-ZnO/i-ZnO/p-SbSSe/n-CdS/Back contact. The simulation is performed using SCAPS-1D software. The optimization process includes optimizing the bulk defect density, bandgap profile, material composition, thickness, and doping density of the absorber layer of thin film solar cell based on antimony selenosulfide $Sb_2(Se_{1-y}S_y)_3$. We found that for a bulk defect density below 10^{13} cm^{-3}, using an absorber material with a graded bandgap profile leads to an efficiency of 25.33 % (For a bulk defect density of 10^{10} cm^{-3}) higher than that with a uniform bandgap profile. However, for a bulk defect density of 10^{13} cm^{-3}, both profiles provide almost the same maximum solar cell conversion efficiencies of about 13.6 %. Ultimately, for a bulk defect density above 10^{13} cm^{-3}, the graded bandgap profile is not useful, and a maximum solar cell conversion efficiency of 10.5 % (For a bulk defect density of 10^{14} cm^{-3}) is achieved with a uniform bandgap profile. These optimization results help to improve the efficiency of low-cost fabricated thin-film solar cells.

(Received December 30, 2023; Accepted April 4, 2024)

Keywords: Antimony selenosulfide $Sb_2(Se_{1-y}S_y)_3$, Thin film solar cell, Graded bandgap, Simulation, Optimization, SCAPS-1D

1. Introduction

Without energy, nothing can work. That is why most countries have given great importance to developing energy in its various forms. These countries tend to move towards renewable energy due to pollution and limited non-renewable energy reserves. Since it is elegant and silent, photovoltaic solar energy is the most used. However, the main drawback that still hinders their exploitation is the cost of solar cells. Therefore, the world's research laboratories aim to increase the conversion efficiency of solar cells while reducing their cost.

On the one hand, this cost can be reduced using less cell absorber material. That is the subject of thin film solar cells such as copper indium gallium diselenide (CIGS), cadmium telluride (CdTe), amorphous silicon (a-Si), and Copper zinc tin sulfo-selenide (CZTSSe) with a record efficiency of 23.6 %, 22.3%, 10.2 % and 14.9 % respectively [1]. Moreover, this cost can also be reduced by using new solar absorber materials composed of earth-abundant, environmentally friendly, and cheaper elements. In this regard, Binary semiconductor compounds in general and metal chalcogenides such as Sb_2Se_3, Sb_2S_3, SnS, PbS, Cu_2S, Ag_2S, Bi_2S_3, FeS_2, $CuSbS_2$, and $CuSbSe_2$, in particular, have attracted a lot of attention because of their suitable optoelectronic properties for thin film solar cells applications [2,3]. Antimony chalcogenides, including Sb_2S_3, Sb_2Se_3, and $Sb_2(Se_{1-y}S_y)_3$ (SbSSe) has recently been identified as a promising candidate for use as absorber material. $Sb_2(Se_{1-y}S_y)_3$ has a high absorption coefficient, good stability, suitable tunable bandgap ranging from 1.18 to 1.63 eV, intrinsically benign grain boundaries, and low melting points [4]. According to Shockley-Queisser limit, the theoretical conversion efficiency of single-junction $Sb_2(Se_{1-y}S_y)_3$ solar cells is 32 % [5].

* Corresponding author: benmir.abdelkader@univ-ouargla.dz
https://doi.org/10.15251/CL.2024.214.305

There are several deposition methods to fabricate the absorber materials for antimony chalcogenide solar cells. The most efficient ones are rapid thermal evaporation, close-spaced sublimation, and spin coating solution process [6]. High efficiencies of 9.2 % and 3.21 % have been obtained for planar-type and sensitized-type Sb_2Se_3 solar cells [7,8]. Whereas, the best efficiencies of planar-type and sensitized-type Sb_2S_3 solar cells are 7.1 % and 7.5 %, respectively [9,10]. A record efficiency of 10.7 %, which is the highest value reported to date for planar-type $Sb_2(Se,S)_3$ solar cells, was reported by Zhao et al. using the hydrothermal deposition method [11].While for the sensitized-type $Sb_2(Se,S)_3$ solar cells reached a record efficiency of 6.6 % [12].

On the other hand, to increase the conversion efficiency of $Sb_2(Se_{1-y}S_y)_3$ solar cells, it is necessary to optimize their parameters. The optimization can be done experimentally or by simulation. Experimental optimization is real, but it is tedious and costly. In addition, we do not have access to some cell parameters. Whereas optimization by simulation is easy, inexpensive and all the cell parameters are accessible.

A review of graded thin-film solar cells can be found in [13]. Many simulation works investigate the effect of the bandgap profile on the performance of thin-film solar cells [14-17]; however, none have linked the bandgap profile to the bulk defect density. That is why, in this work, we will optimize by simulation for each interval of the bulk defect density, the bandgap profile, the material composition, the thickness, and the doping density of the absorber layer of thin film solar cell based on antimony selenosulfide $Sb_2(Se_{1-y}S_y)_3$. The simulation is performed using the latest version 3.3.10 of the numerical software SCAPS-1D, which is a window-based one-dimensional solar cell simulator developed at the University of Gent [18].

2. Simulation model and materials parameters

2.1. Cell structure

As shown in Figure 1, the cell structure used is as follows:

Front contact/n-ZnO/i-ZnO/p-SbSSe/n-CdS/Back contact, such as i-ZnO/n-ZnO as a transparent conductive oxide layer (TCO), cadmium sulfide (CdS) as an n-type buffer layer and SbSSe as a p-type absorber layer.

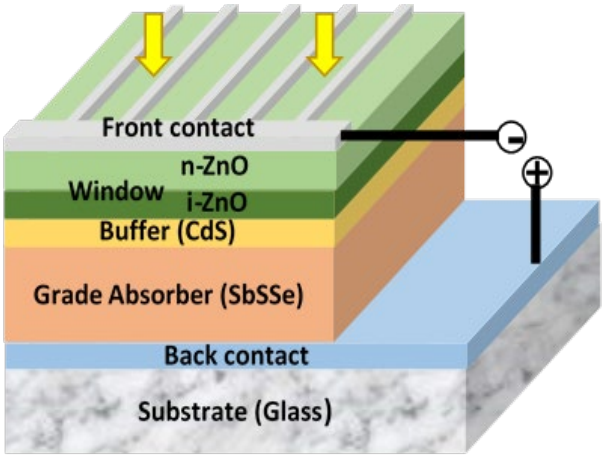

Fig. 1. Schematic diagram of the cell structure used in simulation.

2.2. Simulation software

For the simulation, we used SCAPS software, which solves the three basic equations of semiconductor devices, such as Poisson's equation, the continuity equations and the current density equations for both electrons and holes with appropriate boundary conditions. For the one-dimensional case, under a low-injection condition and at steady state condition, these equations are given by the following equations [19]:

$$div(E) = \frac{\rho(x)}{\varepsilon} \quad (1)$$

$$J_n = q\mu_n nE + qD_n \frac{dn}{dx} \quad (2)$$

$$J_p = q\mu_p pE - qD_p \frac{dp}{dx} \quad (3)$$

$$-\frac{1}{q}\frac{dJ_n}{dx} = G_n - U_n \quad (4)$$

$$\frac{1}{q}\frac{dJ_p}{dx} = G_p - U_p \quad (5)$$

where E, ε and ρ are the electric field, the permittivity and the total electric charge density, respectively; J_n and J_p are the electron current density and the hole current density, respectively; q is the electron charge; n is the electrons concentration in the p-SbSSe layer and p is that of the holes in the n-CdS layer; μ_n and μ_p are the electrons and holes mobility respectively; D_n and D_p are diffusion constant for electrons and holes respectively, which are related to mobility by Einstein's relation ($D = (k.T/q).\mu$); G_n and G_p are the electrons and holes generation rate respectively; U_n and U_p are the electrons and holes recombination rate respectively.

SCAPS has many advantages, such as the ability to simulate up to seven layers with batch and rapidly analyze of the results [20]. In addition, all material parameters can be graded [21]. The results obtained from SCAPS simulator are in good agreement with the experimental results as reported by other researchers [22]. From the output current density–voltage (J–V) characteristics under illumination provided by SCAPS simulation, performance parameters such as *Voc, Jsc, FF,* and η values can be easily obtained. In our simulation, the cell is illuminated from the TCO side (Front contact) with the standard test spectrum AM1.5G, corresponding to a power density of 100 mW/cm^2 for a temperature T = 300 k [23].

2.3. Materials parameters

$Sb_2(Se_{1-y}S_y)_3$ alloy materials can be fabricated with a tunable bandgap because Sb_2S_3 and Sb_2Se_3 are isomorphous semiconductors with the same space group and nearly identical unit-cell parameters [24].

According to Deng et al. [25], the bandgap of $Sb_2Se_{3-z}S_z$ materials is obtained by the following quadratic equation:

$$E_g(z) = 0.0344\, z^2 + 0.0481\, z + 1.18 \text{ eV} \quad (6)$$

Such as $0 \leq z \leq 3$ and $z = 3y$, hence the bandgap of $Sb_2(Se_{1-y}S_y)_3$ materials becomes:

$$E_g(y) = 0.3096\, y^2 + 0.1443\, y + 1.18 \quad (7)$$

where: y = [S]/([S]+[Se]) ratio is the material composition such as $0 \leq y \leq 1$ (See Figure 2).

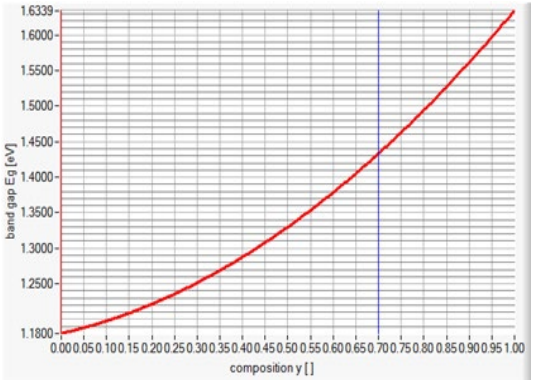

Fig. 2. The band gap $E_g(y)$ as function of composition y in the SbSSe absorber layer (From SCAPS).

The approach followed in SCAPS is materials oriented. Thus, for graded bandgap $Sb_2(Se_{1-y}S_y)_3$ solar cells, it is necessary to introduce the graded profile of the material composition *y(x)* as function of the depth *x* and the composition dependence of all graded material properties including bandgap $E_g(y)$, electron affinity $\chi(y)$, effective density of states $N_C(y)$ and $N_V(y)$, mobility $\mu_n(y)$ and $\mu_p(y)$, dielectric constant $\varepsilon(y)$, and optical absorption $\alpha(\lambda,y)$ [26].

Table 1 groups the properties of each material and interface defects used in the simulation.

Table 1. Materials properties used in the simulation.

Symbols: conduction Band CB, valence Band VB, density of States DOS, donors D, acceptors A, thermal velocity v_{th}, gaussian G, standard energy deviation W_G, peak energy position E_G, electrons e, holes h, capture cross section σ , surface recombination velocity S.

Material properties	n-ZnO	i-ZnO	n-CdS	p-Sb_2Se_3	p-Sb_2S_3	Reference
Layer thickness, d(μm)	0.2	0.05	0.05	Variable	Variable	[16,27,28]
Electron Affinity, χ (eV)	4.45	4.45	4.2	4.15	3.7	[27,29]
Relative permittivity, ε_r	9	9	10	15.1	22	[27,29,30]
Electron mobility, μ_e(cm^2/V.s)	100	100	100	15	9.8	[27,29,30]
Hole mobility, μ_h (cm^2/V.s)	25	25	25	42	10	[27,29,30]
Donor density, N_d (cm^{-3})	1×10^{20}	1×10^{18}	1×10^{17}	-	-	[27]
Acceptor density, N_a (cm^{-3})	-	1×10^{18}	-	Variable	Variable	[27]
Bandgap Energy, E_g (eV)	3.3	3.3	2.4	1.18	1.634	[25,27]
CB effective DOS, N_C(cm^{-3})	2.2×10^{18}	2.2×10^{18}	2.2×10^{18}	1×10^{19}	2×10^{19}	[27,29]
VB effective DOS, N_V(cm^{-3})	1.8×10^{19}	1.8×10^{19}	1.8×10^{19}	1×10^{19}	1×10^{19}	[27,29]
$v_{th,e}$ (cm/s)	10^7	10^7	10^7	10^7	10^7	[16,27,29]
$v_{th,h}$ (cm/s)	10^7	10^7	10^7	10^7	10^7	[16,27,29]
Defects						
Defect type	Single(D)	Single(D)	Single(D)	Single(D)	Single(D)	[29]
Reference	E_v	E_v	E_c	E_i	E_i	[29]
W_{GA}, W_{GD} (eV)	0.1 (D)	0.4 (D)	0.8 (D)	0.1 (A)	0.1 (A)	[29]
E_{GA}, E_{GD} (eV)	1 (D)	1 (D)	1.2 (D)	0.5 (D)	0.5 (D)	[29]
σ_e (cm^2)	1×10^{-14}	1×10^{-14}	3×10^{-15}	3.5×10^{-11}	3.5×10^{-11}	[29]
σ_h (cm^2)	3×10^{-13}	3×10^{-13}	2×10^{-14}	4×10^{-11}	4×10^{-11}	[29]
Defect density, N_t (cm^{-3})	3×10^{16}	1×10^{14}	1×10^{14}	Variable	Variable	[29,30,31,32]
Interface			CdS / SbSSe			
Defect type			Neutral			[31,32]
σ_e (cm^2)			1×10^{-19}			[31,32]
σ_h (cm^2)			1×10^{-19}			[31,32]
Reference for defect energy level E_t			Above the highest E_v			[31,32]
Energy with respect to reference (eV)			0.01			[31,32]
Total density (cm^{-2})			1×10^{10}			[31,32]
Electrodes	Front contact			Back contact		
S_e (cm/s)	10^7			10^7		[16,29]
S_h (cm/s)	10^7			10^7		[16,29]
Work function, Φ_m (eV)	4.45			5.4		[From Scaps]
Reflectivity, R	0.05			0,8		[From Scaps]
General device properties						
Series resistance, R_s (Ω-cm^2)	1.86					[29]
Shunt resistance, R_{sh} (Ω-cm^2)	1600					[29]
Cell temperature, T (K)	300					

3. Results and discussion

It is known that the bulk defect density is linked to the quality of the material and, therefore, to the manufacturing technology of this material. Thus, after several optimization tests by simulation, we have deduced that there are three cases depending on the interval of belonging of the bulk defect density of the solar cell absorber layer. In order to optimize the bandgap profile, each case is further divided into two different cases (Uniform and Graded) as shown in Figure 3. In the case of a uniform bandgap profile, the material composition y is constant along the thickness d. i.e., $\forall\, x \in [0, d]$, $y = y_F = y_B$ = constant Є [0, 1]. Which corresponds - according to Eq. (7) - to a constant bandgap E_g Є[1.18, 1.6339] eV. Whereas, in the case of graded bandgap profile, $\forall\, x \in [0, d]$, $y_F = 0$ and y_B Є [0, 1]. Which corresponds - according to Eq. (7) - to a front bandgap E_{gF} = 1.18 eV and a variable back bandgap E_{gB} Є[1.18, 1.6339] eV. The material composition y is graduated along the thickness d, where it is increased linearly towards the back surface by the following equation:

$$y = \frac{y_B}{d} x \tag{8}$$

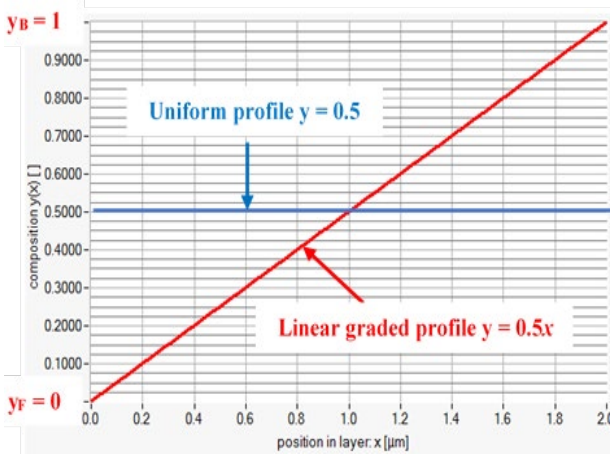

Fig. 3. The material composition y(x) as function of the depth x in the SbSSe absorber layer (Blue line for uniform profile and red line for linear graded profile) (From SCAPS).

For each case of the bandgap profiles, we will first optimize the thickness and the material composition together, and then we will optimize the doping density and the bulk defect density together.

3.1. Low bulk defect density N_t Є $[10^{10}, 10^{12}]$ cm^{-3}

3.1.1. Thickness and bandgap optimization of SbSSe absorber layer

In this case, for each material composition y or y_B Є[0, 1], we vary the thickness d from 0.1 to 2 µm. Figure 4(a) shows the effect of the thickness d and the material composition y (Uniform bandgap profile) of SbSSe absorber layer on the cell performance for $N_a = 10^{18}$ cm^{-3} and $N_t = 10^{10}$ cm^{-3}. According to Eq. (7), if y increases, the bandgap E_g also increases. Therefore, the open circuit voltage increases, and the short circuit current decreases. Hence, the compromise between these two phenomena gives the optimal value of y. It can be seen in Figure 4(a) that for all the values of the thickness d, the maximum efficiency is obtained for an optimum material composition y_{opt} equal to 0.5. Then, if we set the material composition y to this value, we note in Figure 4(a) that the efficiency begins with a rapid increase as the thickness d increases until it becomes almost stable at 24 %, which corresponds to an optimal value d_{opt} around 3 µm. This happens because if the thickness increases, the absorption and, therefore, the generation increases, which increases the short circuit current and consequently increases the conversion efficiency.

Figure 4(b) represents the effect of the thickness d and the back material composition y_B (Graded bandgap profile) of SbSSe absorber layer on the cell performance for $N_a = 10^{18}$ cm^{-3} and $N_t = 10^{10}$ cm^{-3}. Using Eq. (8), we found that on one side, the higher the back material composition y_B, the stronger the additional quasi-electric field and the greater the collection of photo-generated charge carriers and hence the higher the short circuit current [33].

On another side, the higher the back material composition y_B, the lower the absorption of the photons and, therefore, the lower the short circuit current. Furthermore, the higher the back material composition y_B, the higher the open circuit voltage [34]. Therefore, the compromise between these phenomena gives us the optimal value of the back material composition y_B. From Figure 4(b), it can be seen that for each value y_B, if the thickness d increases, the number of photo-generated charge carriers increases. Which increases the short circuit current and, subsequently, the conversion efficiency. However, due to the recombination process, the short circuit current and the conversion efficiency reach a saturation level corresponding to the optimum thickness d_{opt}. The smallest optimal values giving a maximum conversion efficiency of 25.33 % are $y_{Bopt} = 0.7$ [35] and $d_{opt} = 1.4$ µm [17]. Whereas the largest optimal values with the same conversion efficiency are $y_{Bopt} = 1$ and $d_{opt} = 2$ µm.

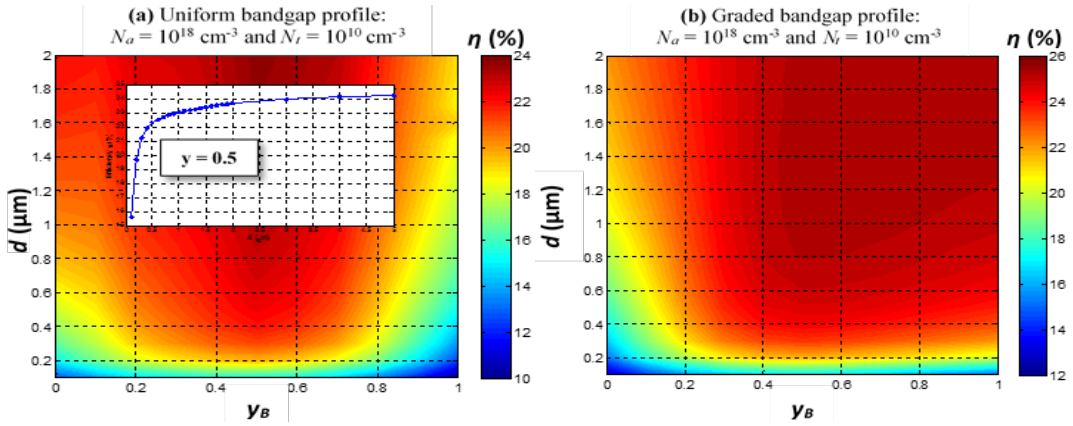

Fig. 4. Contour plot of solar cell efficiency η as a function of the thickness and the material composition of SbSSe absorber layer for: (a) Uniform bandgap profile (b) Graded bandgap profile.

By comparing Figure 4(a) and Figure 4(b), we conclude that the conversion efficiency of the solar cell with a graded bandgap profile is higher than that with a uniform bandgap profile. This is because the graded bandgap profile creates an additional quasi-electric field which improves the collection of the photo-generated charge carriers and therefore the short circuit current is enhanced.

3.1.2. Doping density and bulk defect density optimization of SbSSe absorber layer

In this case, we fix the bulk defect density N_t at a value in the interval [10^{10}, 10^{12}] cm^{-3}, and then, we change the value of the doping density N_a in the interval [10^{12}, 10^{18}] cm^{-3}. Figure 5(a) illustrates the effect of the doping density N_a and the bulk defect density N_t of SbSSe absorber layer on the cell performance for $d_{opt} = 3$ µm and $y_{opt} = 0.5$ (uniform bandgap profile).

It is observed that for a fixed doping density, if the bulk defect density increases, the lifetime and, subsequently, the diffusion length decrease, which leads to a decrease in the collection of charge carriers and, thus, in the conversion efficiency. However, for a constant bulk defect density, the higher the doping density, the greater the conversion efficiency. This explains that if the doping density increases, the conductivity also increases, and therefore the series resistance decreases, which leads to an increase in the fill factor. Moreover, the open circuit voltage is improved by the increase in doping density [36]. Although the width of the space charge region on the absorber layer side w_p is reduced, which decreases the collection of photo-generated charge carriers and, thus, the short circuit current. Consequently, a maximum conversion

efficiency of 24 % is obtained for the following four optimal values: y_{opt} = 0.5 (Uniform bandgap profile), d_{opt} = 3µm, N_{topt} = 10^{10} cm^{-3} and N_{aopt} = 10^{18} cm^{-3}. This implies that the open circuit voltage and the fill factor predominate the variation of the conversion efficiency. These results are in good agreement with [36].

Figure 5(b) shows the effect of the doping density and the bulk defect density of SbSSe absorber layer on the cell performance for d_{opt} = 1.4 µm and y_{Bopt} = 0.7 (Graded bandgap profile). The interpretation is the same as in the case of the uniform bandgap profile. The difference is that thanks to the additional quasi-electric field generated by the graded bandgap profile, we observe that the solar cell conversion efficiency of the graded bandgap profile in Figure 5(b) is greater than that of the uniform bandgap profile in Figure 5(a). As a result, a maximum conversion efficiency of 25.33 % is reached for the following four optimal values: y_{Bopt} = 0.7 (Graded bandgap profile), d_{opt} = 1.4 µm, N_{topt} =10^{10} cm^{-3} and N_{aopt} = 10^{18} cm^{-3}.

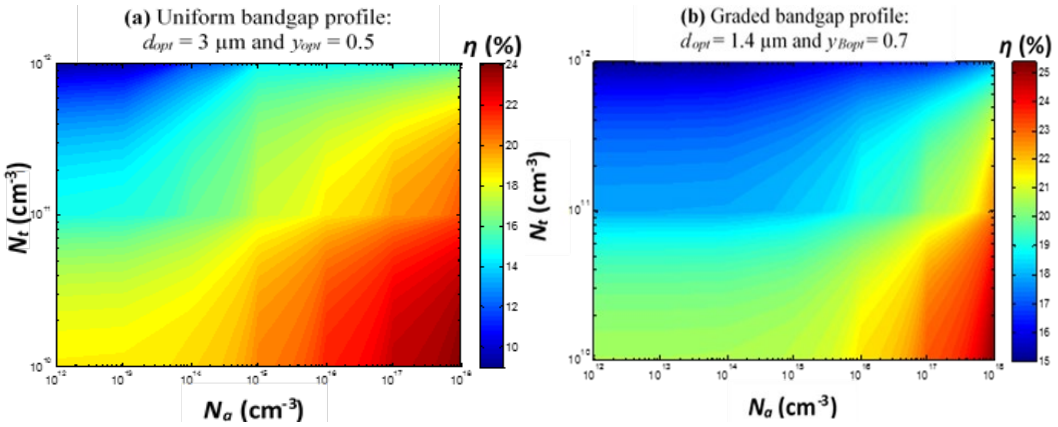

Fig. 5. Contour plot of solar cell efficiency as a function of the doping density and the bulk defect density of SbSSe absorber layer for: (a) Uniform bandgap profile (b) Graded bandgap profile.

3.2. Medium bulk defect density N_t = 10^{13} cm^{-3}

3.2.1. Thickness and bandgap optimization of SbSSe absorber layer

Figure 6(a) represents the effect of the thickness d and the material composition y (Uniform bandgap profile) of SbSSe absorber layer on the cell performance for N_a = 10^{16} cm^{-3} and N_t = 10^{13} cm^{-3}. We know that the bandgap E_g increases when y increases. Consequently, the trade-off between reducing the short circuit current and increasing the open-circuit voltage gives the optimum value of y. So it appears from Figure 6(a) that, for a constant thickness d, the maximum efficiency is obtained for an optimum material composition y_{opt} equal to 0 (Sb_2Se_3). This means that the short circuit current predominates the variation of the conversion efficiency. However, if the absorber layer thickness d increases, the number of photo-generated charge carriers increases. This results in an increase in the short circuit current. But, due to the relatively high defect density, which leads to low conductivity, if the thickness d increases, its series resistance also increases. Consequently, the fill factor is reduced. Hence for y_{opt} = 0 we deduce in Figure 6(a) an optimal value of the thickness d_{opt} equal to 0.3 µm [17] giving a maximum efficiency of 13.58 %.

Figure 6(b) illustrates the effect of the thickness d and the back material composition y_B (Graded bandgap profile) of SbSSe absorber layer on the cell performance for N_a = 10^{18} cm^{-3} and N_t = 10^{13} cm^{-3}. According to Eq. (8), we found that, on the one hand, the higher the back material composition y_B, the higher the open circuit voltage and the lower the short circuit current. On the other hand, for high values of y_B, the decrease in the short circuit current is compensated by an increase caused by the intense additional quasi-electric field. Therefore, it is evident in Figure 6(b) that the optimal value of the back material composition is the largest value y_{Bopt} = 1. This means that the open circuit voltage predominates the variation in the conversion efficiency. However, if the absorber layer thickness d increases, the short circuit current increases, and due to the relatively high defect density the fill factor decreases.

As a result, from Figure 6(b) for y_{Bopt} = 1 (Graded bandgap profile), we can extract an optimal value of the thickness d_{opt} equal to 0.3 µm giving a maximum efficiency of 13.72 %. By comparing Figure 6(a) with Figure 6(b), we conclude that the maximum solar cell conversion efficiencies for both profiles (Graded and uniform) are almost equal.

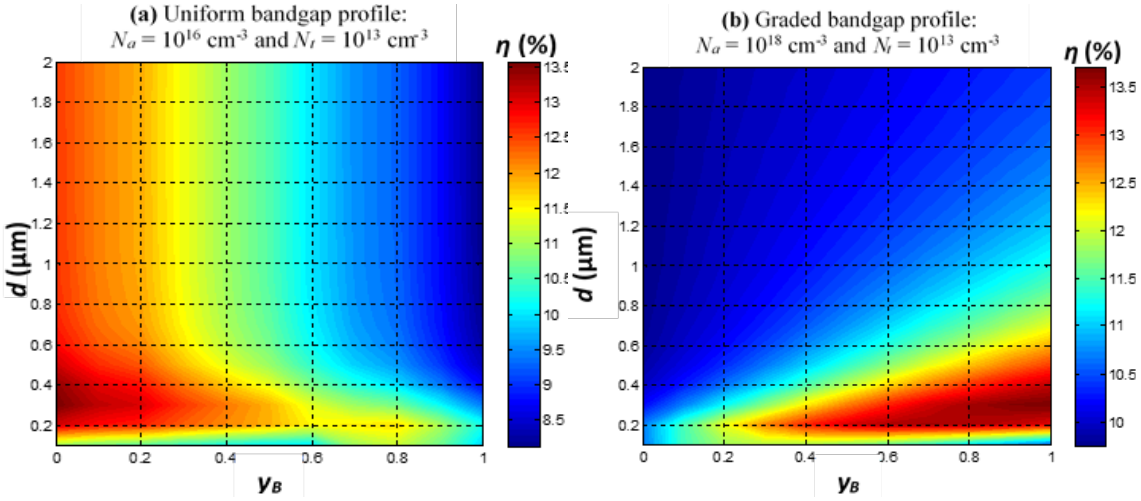

Fig. 6. Contour plot of solar cell efficiency η as a function of the thickness and the material composition of SbSSe absorber layer for: (a) Uniform bandgap profile (b) Graded bandgap profile.

3.2.2. Doping density and bulk defect density optimization of SbSSe absorber layer

Figure 7(a) shows the effect of the doping density of SbSSe absorber layer on the cell performance for d_{opt} = 0.3 µm, y_{opt} = 0 (Uniform bandgap profile) and $N_t = 10^{13}$ cm^{-3}. Whereas, Figure 7(b) represents the effect of the doping density of SbSSe absorber layer on the cell performance for d_{opt} = 0.3 µm, y_{Bopt} = 1 (Graded bandgap profile) and $N_t = 10^{13}$ cm^{-3}. It is known, according to the electrical neutrality equation, that the width of the space charge region on the absorber layer side w_p decreases with increasing doping density N_a of this layer and vice versa. We notice in Figure 7 (a)-(b) that if N_a is less than or equal to 10^{16} cm^{-3}, w_p is greater than the thickness d of the absorber layer. In this case, the short circuit current and accordingly the conversion efficiency are invariable. But, when N_a is greater than 10^{16} cm^{-3}, w_p is less than d, which improves the fill factor and the open circuit voltage. Furthermore, the short circuit current is reduced by the decrease of the collection of photo-generated charge carriers. Hence, the conversion efficiency is decreased in Figure 7(a). This implies that the short circuit current predominates the variation of the conversion efficiency.

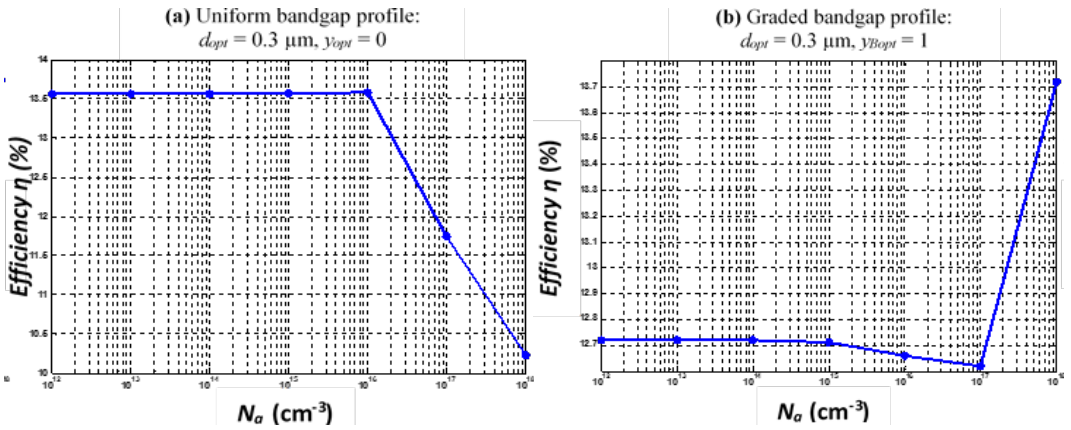

Fig. 7. Contour plot of solar cell efficiency as a function of the doping density of SbSSe absorber layer for: (a) Uniform bandgap profile (b) Graded bandgap profile.

On the other hand, in Figure 7(b), the reduction of the short circuit current is compensated by an increase caused by the high additional quasi-electric field. This compensation increases the conversion efficiency (contrary to the uniform bandgap profile) to: 12.62 % for $N_a = 10^{17}$ cm^{-3} and 13.72 % for $N_a = 10^{18}$ cm^{-3}. This implies that the open circuit voltage and the fill factor predominate the variation of the conversion efficiency.

The comparison between Figure 7(a) and Figure 7(b) allows us to deduce that for $N_a \leq 10^{16}$ cm^{-3}, the solar cell conversion efficiency with a uniform bandgap profile is higher than that with a graded bandgap profile. While for $N_a > 10^{16}$ cm^{-3}, the solar cell conversion efficiency with a graded bandgap profile is superior to that with a uniform bandgap profile. As a result, for SbSSe absorber material with a bulk defect density of 10^{13} cm^{-3}, we can choose one or the other of the two profiles. Where for a uniform bandgap profile, a maximum conversion efficiency of 13.58 % is reached for the following three optimal values: $y_{opt} = 0$ (Sb_2Se_3), $d_{opt} = 0.3$ µm and $N_{aopt} \leq 10^{16}$ cm^{-3}. While for a graded bandgap profile, a maximum conversion efficiency of 13.72 % is achieved for the following three optimal values: $y_{Bopt} = 1$, $d_{opt} = 0.3$ µm and $N_{aopt} = 10^{18}$ cm^{-3}.

3.3. High bulk defect density $N_t \in [10^{14}, 10^{16}]$ cm^{-3}

3.3.1. Thickness and bandgap optimization of SbSSe absorber layer

Figure 8(a) illustrates the effect of the thickness d and the material composition y (Uniform bandgap profile) of SbSSe absorber layer on the cell performance for $N_a = 10^{16}$ cm^{-3} and $N_t = 10^{14}$ cm^{-3}. As we know, the bandgap increases with increasing material composition y. Therefore, the lower the material composition y, the lower the open circuit voltage. However, the lower the material composition y, the higher the short circuit current. Thus, there is a compromise that produces the optimal value of y. Hence, similar to § 3.2.1, it can be seen from Figure 8(a) that if the material composition y increases, the conversion efficiency decreases with a high decrease rate up to a minimum value (As an example, for $d = 0.2$ µm, the conversion efficiency decreases from 10.5 % to 4.6 %). As a result, for each value of the thickness d, the maximum efficiency is obtained for an optimum material composition y_{opt} equal to 0 (Sb_2Se_3). This means that the short circuit current's contribution to affecting the solar cell's performance is more significant than the open circuit voltage.

On the other side, increasing the thickness d of the absorption layer increases the number of photo-generated charge carriers. Consequently, the short circuit current increases. However, due to the high defect density, which leads to low conductivity, increasing the thickness d of the absorber layer increases its series resistance. Accordingly, the fill factor is reduced.

As a result, for y_{opt} equal to 0, the conversion efficiency reaches its maximum $\eta = 10.5$ % for an optimal value of the absorber layer thickness equal to 0.2 µm. It can also be seen that the conversion efficiency is almost constant for all values of the thickness d exceeding 0.3 µm.

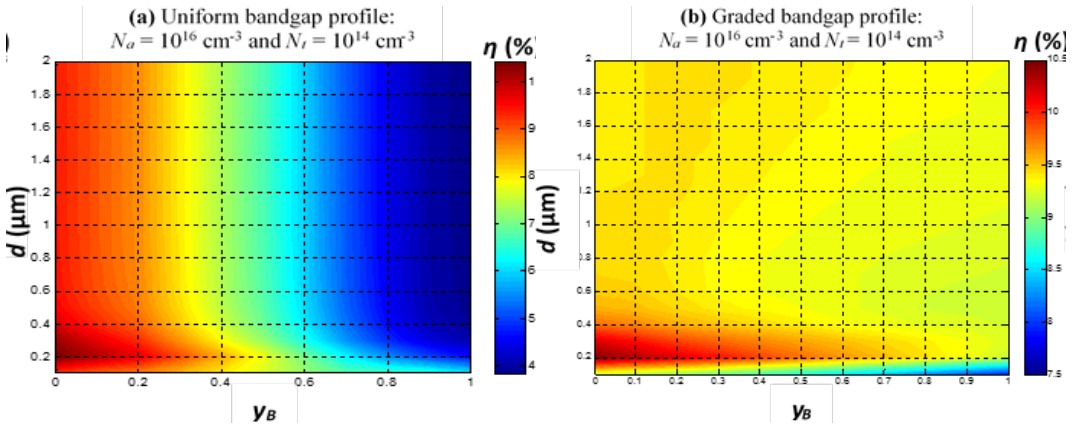

Fig. 8. Contour plot of solar cell efficiency η as a function of the thickness and the material composition of SbSSe absorber layer for: (a) Uniform bandgap profile (b) Graded bandgap profile.

Figure 8(b) shows the effect of the thickness d and the back material composition y_B (Graded bandgap profile) of SbSSe absorber layer on the cell performance for $N_a = 10^{16}$ cm^{-3} and $N_t = 10^{14}$ cm^{-3}. Similar to the case of the uniform bandgap profile, if the material composition y_B increases, the conversion efficiency decreases but with a weak decrease rate up to a minimum value (As an example, for $d = 0.2$ µm, the conversion efficiency decreases from 10.5 % to 9.2 %). On the other hand, if absorber layer thickness d increases, the conversion efficiency increases to reach its maximum $\eta = 10.5$ % for an optimal value of the absorber layer thickness $d_{opt} = 0.2$ µm. But as soon as d exceeds this value, the efficiency decreases to reach a saturation level where it becomes almost constant.

Comparing Figure 8(a) and Figure 8(b), we conclude that, owing to the additional quasi-electric field generated by the graded bandgap profile, for all absorber materials $Sb_2(Se_{1-y}S_y)_3$ with $y \neq 0$, the conversion efficiency of the graded bandgap profile (y_B) is greater than that of the uniform bandgap profile ($y = y_B$). In addition, the higher the back material composition y_B, the more significant the difference between the conversion efficiency of the graded bandgap profile (y_B) and that of the uniform bandgap profile ($y = y_B$). But, the conversion efficiency of absorber material with uniform bandgap profile $y = 0$ (Sb_2Se_3) is greater than that of any other absorber material $Sb_2(Se_{1-y}S_y)_3$ with graded bandgap profile ($y_B \neq 0$). Consequently, in this case, we deduce that the graded bandgap profile is not beneficial.

3.3.2. Doping density and bulk defect density optimization of SbSSe absorber layer

Figure 9 illustrates the effect of the doping density and bulk defect density of SbSSe absorber layer on the cell performance for $d_{opt} = 0.2$ µm and $y_{opt} = 0$ (Uniform bandgap profile). We know that if the bulk defect density increases, the lifetime and the diffusion length decrease. This leads to a decrease in the collection of photo-generated charge carriers and an increase in their recombination. Which reduces the short circuit current and, subsequently, the conversion efficiency, as shown in Figure 9. It can be seen from Figure 9 that, as long as N_a does not exceed 10^{16} cm^{-3}, w_p is greater than the thickness d of the absorber layer. This means that N_a does not influence the collection of photo-generated charge carriers. Thus the short circuit current and the conversion efficiency are constant. But, as soon as N_a exceeds the value 10^{16} cm^{-3}, w_p is less than d. This reduces the collection of photo-generated charge carriers, and accordingly, the short circuit current and the conversion efficiency are thereby reduced. We also concluded that the short circuit current predominates the variation of the conversion efficiency.

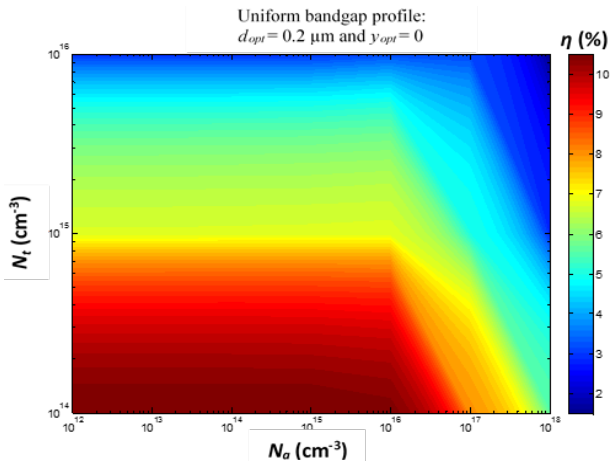

Fig. 9. Contour plot of solar cell efficiency as a function of the doping density and the bulk defect density of SbSSe absorber layer for Uniform bandgap profile.

Consequently, a maximum conversion efficiency of 10.5 % is obtained for the following four optimal values: $y_{opt} = 0$ (Uniform bandgap profile), $d_{opt} = 0.2$ µm, $N_{topt} = 10^{14}$ cm^{-3} and $N_{aopt} \leq 10^{16}$ cm^{-3}. These results are in agreement with [7].

4. Conclusion

In this work, we carried out an optimization by simulation of a graded bandgap thin film solar cell based on antimony selenosulfide $Sb_2(Se_{1-y}S_y)_3$ having the following structure: Front contact/n-ZnO/i-ZnO/p-SbSSe/n-CdS/ Back contact. The optimization is performed using simulation with the software SCAPS-1D, where for each interval of the bulk defect density, we optimize the bandgap profile, the thickness, and the doping density of the $Sb_2(Se_{1-y}S_y)_3$ absorber layer of the solar cell. The obtained results showed that for a low bulk defect density $N_t \in [10^{10}, 10^{12}]$ cm^{-3}, thanks to the additional quasi-electric field generated by the graded bandgap profile, the solar cell conversion efficiency for absorber with graded bandgap profile is more significant than that with uniform bandgap profile. For the uniform bandgap profile, a maximum conversion efficiency of 24 % is obtained for the following four optimal values: y_{opt} = 0.5, d_{opt} = 3 µm, $N_{topt}=10^{10}$ cm^{-3} and N_{aopt} = 10^{18} cm^{-3}. Whereas, for the graded bandgap profile, a maximum conversion efficiency of 25.33 % is reached for the following four optimal values: y_{Bopt} = 0.7, d_{opt} = 1.4 µm, N_{topt} = 10^{10} cm^{-3} and N_{aopt} = 10^{18} cm^{-3}.

However, for a medium bulk defect density N_t = 10^{13} cm^{-3}, we constated that for $N_a \leq 10^{16}$ cm^{-3}, the solar cell conversion efficiency for an absorber with a uniform bandgap profile is higher than that with a graded bandgap profile. While, for $N_a > 10^{16}$ cm^{-3}, the solar cell conversion efficiency for absorber with a graded bandgap profile is superior to that with a uniform bandgap profile. Therefore, we can choose one or the other of the two profiles. For the uniform bandgap profile, a maximum conversion efficiency of 13.58 % is reached for the following three optimal values: y_{opt} = 0 (Sb_2Se_3), d_{opt} = 0.3 µm and $N_{aopt} \leq 10^{16}$ cm^{-3}. While for the graded bandgap profile, a maximum conversion efficiency of 13.72 % is achieved for the following three optimal values: y_{Bopt} = 1, d_{opt} = 0.3 µm and N_{aopt} = 10^{18} cm^{-3}.

Finally, for a high bulk defect density $N_t \in [10^{14}, 10^{16}]$ cm^{-3}, we have demonstrated that the absorber layer's doping density must have a value at most equal to 10^{16} cm^{-3}. We have also found that, owing to the additional quasi-electric field generated by the graded bandgap profile, for all absorber materials $Sb_2(Se_{1-y}S_y)_3$ with $y \neq 0$, the solar cell conversion efficiency for absorber with graded bandgap profile (y_B) is greater than that with uniform bandgap profile ($y = y_B$).

On the contrary, the solar cell conversion efficiency for absorber material with uniform bandgap profile y = 0 (Sb_2Se_3) is greater than that for absorber material $Sb_2(Se_{1-y}S_y)_3$ with graded bandgap profile ($y_B \neq 0$). Hence, we have deduced that the graded bandgap profile is not beneficial in this case. Consequently, a maximum conversion efficiency of 10.5 % is obtained for the following four optimal values: y_{opt} = 0, d_{opt} = 0.2 µm, N_{topt} = 10^{14} cm^{-3} and $N_{aopt} \leq 10^{16}$ cm^{-3}.

These optimization results confirm the promising prospects for improving the efficiency of fabricated low-cost thin film solar cells.

Acknowledgements

The authors would like to thank Professor Marc Burgelman of Gent University, Belgium, for providing the SCAPS program.

References

[1] M. A. Green, E. D. Dunlop, M. Yoshita, N. Kopidakis, K. Bothe, G. Siefer, X. Hao, Progress in Photovoltaics: Research and Applications, **32**(1), 3 (2023); https://doi.org/10.1002/pip.3726
[2] D. G. Moon, S. Rehanb, D. H. Yeon, S. M. Lee, S. J. Park, S. Ahn, Y. S. Cho, Solar Energy Materials and Solar Cells, **200,** 109963 (2019); https://doi.org/10.1016/j.solmat.2019.109963
[3] K. Zeng, D-J. Xue, J. Tang, Semiconductor Science and Technology, **31**(6), 063001 (2016); https://iopscience.iop.org/article/10.1088/0268-1242/31/6/063001
[4] X. Wang, R. Tang, C. Wu, C. Zhu, T. Chen, Journal of Energy Chemistry, **27**(3), 713 (2018); https://doi.org/10.1016/j.jechem.2017.09.031

[5] W. Shockley, H. J. Queisser, Journal of Applied Physics, **32**(3), 510 (1961); https://doi.org/10.1063/1.1736034
[6] A. Mavlonov, T. Razykov, F. Raziq, J. Gan, J. Chantana, Y. Kawano, T. Nishimura, H. Wei, A. Zakutayev, T. Minemoto, X. Zu, S. Li, L. Qiao, Solar Energy, **201,** 227 (2020); https://doi.org/10.1016/j.solener.2020.03.009
[7] Z. Li, X. Liang, G. Li, H. Liu, H. Zhang, J. Guo, J. Chen, K. Shen, X. San, W. Yu, R. E. I. Schropp, Y. Mai, Nature Communications, **10,** 125 (2019); https://doi.org/10.1038/s41467-018-07903-6
[8] Y. C. Choi, T. N. Mandal, W. S. Yang, Y. H. Lee, S.H. Im, J. H. Noh, S. I. Seok, Angewandte Chemie, **126**(5), 1353 (2014); https://doi.org/10.1002/ange.201308331
[9] J. Han, S. Wang, J. Yang, S. Guo, Q. Cao, H. Tang, X. Pu, B. Gao, X. Li, ACS Applied Materials & Interfaces, **12**(4), 4970 (2020) ; https://pubs.acs.org/doi/10.1021/acsami.9b15148
[10] Choi Y C, Lee D U, Noh J H, Kim E K and Seok S I, Advanced Functional Materials, **24**(23), 3587 (2014); https://doi.org/10.1002/adfm.201304238
[11] Y. Zhao, S. Wang, C. Jiang, C. Li, P. Xiao, R. Tang, J. Gong, G. Chen, T. Chen, J. Li, X. Xiao, Advanced Energy Materials, **12**(1)**,** 2103015 (2022); https://doi.org/10.1002/aenm.202103015
[12] Y. C. Choi, Y. H. Lee, S. H. Im, J. H. Noh, T. N. Mandal, W. S. Yang, S. I. Seok, Advanced Energy Materials, **4**(7), 1301680 (2014); https://doi.org/10.1002/aenm.201301680
[13] I. Sharma, P. S. Pawar, R. K. Yadav, R. Nandi, J. Heo, Solar Energy, **246,** 152 (2022); https://doi.org/10.1016/j.solener.2022.09.046
[14] I. Gharibshahian, A. A. Orouji, S. Sharbati, Solar Energy, **227,** 606 (2021); https://doi.org/10.1016/j.solener.2021.09.039
[15] M. Wu, N. Han, Y. Chen, H. Zeng, X. Li, Optik, **272,** 170393 (2023); https://doi.org/10.1016/j.ijleo.2022.170393
[16] M. T. Islam, A. K. Thakur, Solar Energy, **202,** 304 (2020); https://doi.org/10.1016/j.solener.2020.03.058
[17] T. Jiménez, D. Seuret-Jiménez, O. Vigil-Galán, M. A. Basurto-Pensado, M. Courel, Journal of Physics D: Applied Physics, **51**(43)**,** 435501 (2018); https://doi.org/10.1088/1361-6463/aaddea
[18] M. Burgelman, P. Nollet, S. Degrave, Thin Solid Films, **361-362**, 527 (2000); https://doi.org/10.1016/S0040-6090(99)00825-1
[19] S. M. Sze, Physics of Semiconductor Devices, Wiley, New York, (1981);
[20] Mamta, K. K. Maurya, V. N. Singh, Solar Energy, **228,** 540 (2021); https://doi.org/10.1016/j.solener.2021.09.080
[21] A. Haddout, M. Fahoume, A. Qachaou, A. Raidou, M. Lharch, N. Elharfaoui, Solar Energy, **189,** 491 (2019); https://doi.org/10.1016/j.solener.2019.07.098
[22] L. Et-taya, T. Ouslimane, A. Benami, Solar Energy, **201,** 827 (2020); https://doi.org/10.1016/j.solener.2020.03.070
[23] S. J. Fonash, "Solar Cell Device Physics", Elsevier, Oxford, (2010); https://doi.org/10.1016/C2009-0-19749-0
[24] H. Lei, J. Chen, Z. Tan, G. Fang, Solar RRL, **3**(6), 1900026 (2019); https://doi.org/10.1002/solr.201900026
[25] Z, Deng, M, Mansuripur, A. J. Muscat, Nano Letters, **9**(5)**,** 2015 (2009); https://doi.org/10.1021/nl9002816
[26] M. Burgelman, K. Decock, S. Khelifi, A. Abass, Thin Solid Films, **535,** 296 (2013); https://doi.org/10.1016/j.tsf.2012.10.032
[27] A. Basak, U. P. Singh, Solar Energy Materials and Solar Cells, **230,** 111184 (2021); https://doi.org/10.1016/j.solmat.2021.111184
[28] M. Courel, T. Jiménez, A. Arce-Plaza, D. Seuret-Jiménez, J. P. Morán-Lázaro, F. J. Sánchez-Rodríguez, Solar Energy Materials and Solar Cells, **201,** 110123 (2019); https://doi.org/10.1016/j.solmat.2019.110123
[29] I. Gharibshahian, A. A. Orouji, S. Sharbati, Solar Energy Materials and Solar Cells, **212,** 110581 (2020); https://doi.org/10.1016/j.solmat.2020.110581
[30] J. Dong, Y. Liu, Z. Wang, Y. Zhang, Nano Select, **2**(10), 1818 (2021); https://doi.org/10.1002/nano.202000288

[31] A. Sunny, S. R. A. Ahmed, physica Status Solidi B, **258**(7), 2000630 (2021); https://doi.org/10.1002/pssb.202000630
[32] S. R. A. Ahmed, A. Sunny, S. Rahman, Solar Energy Materials and Solar Cells, **221,** 110919 (2021); https://doi.org/10.1016/j.solmat.2020.110919
[33] A. Belghachi, N. Limam, Chinese Journal of Physics, **55**(4), 1127 (2017); https://doi.org/10.1016/j.cjph.2017.01.011
[34] T. Dullweber, G. Hanna, W. Shams-Kolahi, A. Schwartzlander, M. A. Contreras, R. Noufi, H. W. Schock, Thin Solid Films, **361-362,** 478 (2000); https://doi.org/10.1016/S0040-6090(99)00845-7
[35] R. Tang, X. Wang, W. Lian, J. Huang, Q. Wei, M. Huang, Y. Yin, C. Jiang, S. Yang, G. Xing, S. Chen, C. Zhu, X. Hao, M. A. Green, T. Chen, Nature Energy, **5,** 587 (2020); https://doi.org/10.1038/s41560-020-0652-3
[36] Z. Ali, K. Ali, B. Hussain, S. Maqsood. I. Iqbal, Optical Materials, **128,** 112358 (2022); https://doi.org/10.1016/j.optmat.2022.112358